JMEPEG (2016) 25:1931–1938
DOI: 10.1007/s11665-016-2006-7

1059-9495/$19.00

Effects of Recrystallization on Microstructure and Texture Evolution of Cold-Rolled Ti-6Al-4V Alloy

Haitao Jiang, Peng Dong, Shangwu Zeng, and Bo Wu

(Submitted June 10, 2015; in revised form January 23, 2016; published online April 8, 2016)

The effects of recrystallization during annealing process on microstructure and texture evolution of cold-rolled Ti-6Al-4V alloy plates were investigated. The plates after cold rolling with a thickness reduction of 5, 10, and 15% were annealed under different conditions of 750 °C for 1 h, 800 °C for 1 h, and 800 °C for 1.5 h, respectively. It was found out that the recrystallization temperature decreased with increasing rolling reduction due to higher storage energy, while the extension of annealing time caused grain growth. For the cold-rolled plate with a reduction of 10%, the resulting microstructure showed more equal-axis grains after annealing at 800 °C for 1 h, among different conditions. Moreover, the XRD results showed that the cold-rolled plate composed mainly of {0001} ⟨10-10⟩ basal texture, {10-11} ⟨1-210⟩ and {01-12} ⟨10-10⟩ pyramidal textures, and {01-10} ⟨10-10⟩ prismatic texture, and that the weak {10-11} ⟨1-210⟩ texture was transformed to components {01-12} ⟨10-10⟩ and {01-10} ⟨10-10⟩, which were expected to improve formability. Electron back-scattered diffraction results ascertained that two mechanisms, i.e., recrystallization sites of preferred orientations and favorable grain growth both played important roles in static recrystallization.

Keywords advanced characterization, heat treatment, microscopy, optical metallography, rolling, titanium, x-ray

1. Introduction

According to the phase nature at room temperature, titanium alloy can be classified into three types, i.e., α and near-α alloys, α/+β alloys, and β alloys (Ref 1-3). Because of their low density, high strength-to-weight ratio, and outstanding comprehensive performance, titanium alloy tubes face an increasing demand from aeronautics and astronautics, automotive, shipbuilding, and energy industries (Ref 4). Among titanium alloys, widely used Ti-6Al-4V alloy is an excellent candidate for manufacturing titanium alloy tubes (Ref 5, 6), especially applied to aerospace and oil industry. In general, the main manufacturing process of Ti-6Al-4V alloy tubes includes hot rolling, drawing, and Helical bar piercing, mostly for thick wall tubes. Although a clear record of thin wall tubes via hot rolling has been confirmed, complicated equipment and process as well as high product cost restricts its mass production. Titanium alloy tubes with low strength or low alloy content can be produced through cold rolling, during which metal consumption can be reduced (Ref 7). However, the smooth production and the uniformity requirement are challenges to the cold-rolled tubes with moderate strength especially for thin tubes due to their high resistance to deformation (Ref 8). Ti-6Al-4V alloy is easily to be deformed by hot rolling to improve microstructures and subsequent cold rolling is carried out to enhance surface quality and dimensional precision. Therefore, it is necessary to clarify the micromechanism of how the rolling and subsequent annealing processes affect mechanical properties of Ti-6Al-4V tube.

Many researches have been conducted on the influences of rolling and annealing parameters on microstructures, texture evolution and mechanical properties. Chun et al. studied the effects of deformation twinning and slip on grain refinement in a commercial-purity titanium (CP-Ti) in which both compressive ({11-22} ⟨11-2-3⟩) and tensile ({10-12} ⟨10-11⟩) twins as well as secondary twins and tertiary twins were activated to form heterogeneous microstructures (Ref 9). But the effects of recrystallization on texture evolution during annealing as well as the basic properties were not mentioned. Huang and Yuasa noticed a dramatic change in the rolling texture during differential speed rolling (DSR), from the transverse direction (TD) split texture with basal poles largely tilted at ±40° to the single-peak basal texture (Ref 10). Peng et al. analyzed effects of β treatments on microstructures and properties of the Ti-6Al-4V alloy, and the results showed that microstructures were lamellar after processing and acicular Widmanstatten after annealing, respectively (Ref 11). Carreon researched the direct correlation between tensile ductility and the presence of a preferred crystallographic orientation of polycrystalline microstructure of rolled Ti-6Al-4V alloy annealed at 710°C for 2 h using thermoelectric power measurements (Ref 12), but detailed textures were not presented. So it is crucial to determine the influence of static recrystallization during annealing on the microstructures and textures of cold-rolled Ti-6Al-4V alloy. In this paper, light deformation combined with annealing was designed to simulate the production of titanium alloy tube, in order to explore rules of recrystallization process and texture evolution.

2. Experimental

The material used in this work was typical Ti-6Al-4V alloy received as forged ingot after hot rolling with the dimensions of

Haitao Jiang, Peng Dong, Shangwu Zeng, and **Bo Wu**, National Engineering Research Center for Advanced Rolling Technology, University of Science and Technology Beijing, Beijing 100083, China. Contact e-mail: jianght@ustb.edu.cn.

380 mm×81 mm×41 mm, which was cut to plates with dimensions of 380 mm × 81 mm × 4 mm. The microstructure of the forged ingot exhibited a fully homogeneous equiaxed structure with an average grain size of 9.2 μm. The plates were cold rolled at room temperature with a total thickness reduction of 5, 10, and 15%, respectively, with the thickness being reduced by 0.2 mm after each pass in a four-high reversing mill at a speed of 0.04 m/s. Thereafter, the cold-rolled plates were annealed under different conditions, namely 750 °C for 1 h, 800 °C for 1 h and 800°C for 1.5 h, respectively, followed by air cooling to room temperature.

The microstructures of the as-received material as well as the cold-rolled and annealed plates were observed by optical microscope (OM). Average grain size of α and β phases were determined using optical metallography via a linear intercept method, and the edge grains were excluded from the measurement scheme. Furthermore, a D8 advanced x-ray diffractometer (XRD) was introduced to analyze the influence of recrystallization on texture evolution by pole figure (PF) and orientation distribution function (ODF) was calculated by five pole figures ((0002), (10-10), (10-11), (10-12), and (11-20)). From the ODFs, complete pole figures were reconstructed. The rectangular specimens in 25 mm × 20 mm for XRD test were cut along the rolling direction (RD). The specimens subjected to annealing were cut into specimens in 6 mm × 4 mm along rolling direction, and misorientation angle distribution was analyzed by a ZEISS SUPRA 55 thermal field emission scanning electron microscope with an electron back-scattered diffraction (EBSD) system.

3. Results and Discussion

3.1 Microstructure

The optical microstructures of the cold-rolled Ti-6Al-4V alloy are shown in Fig. 1. The microstructures of Ti-6Al-4V alloy after cold rolling consisted of α matrix and intergranular β

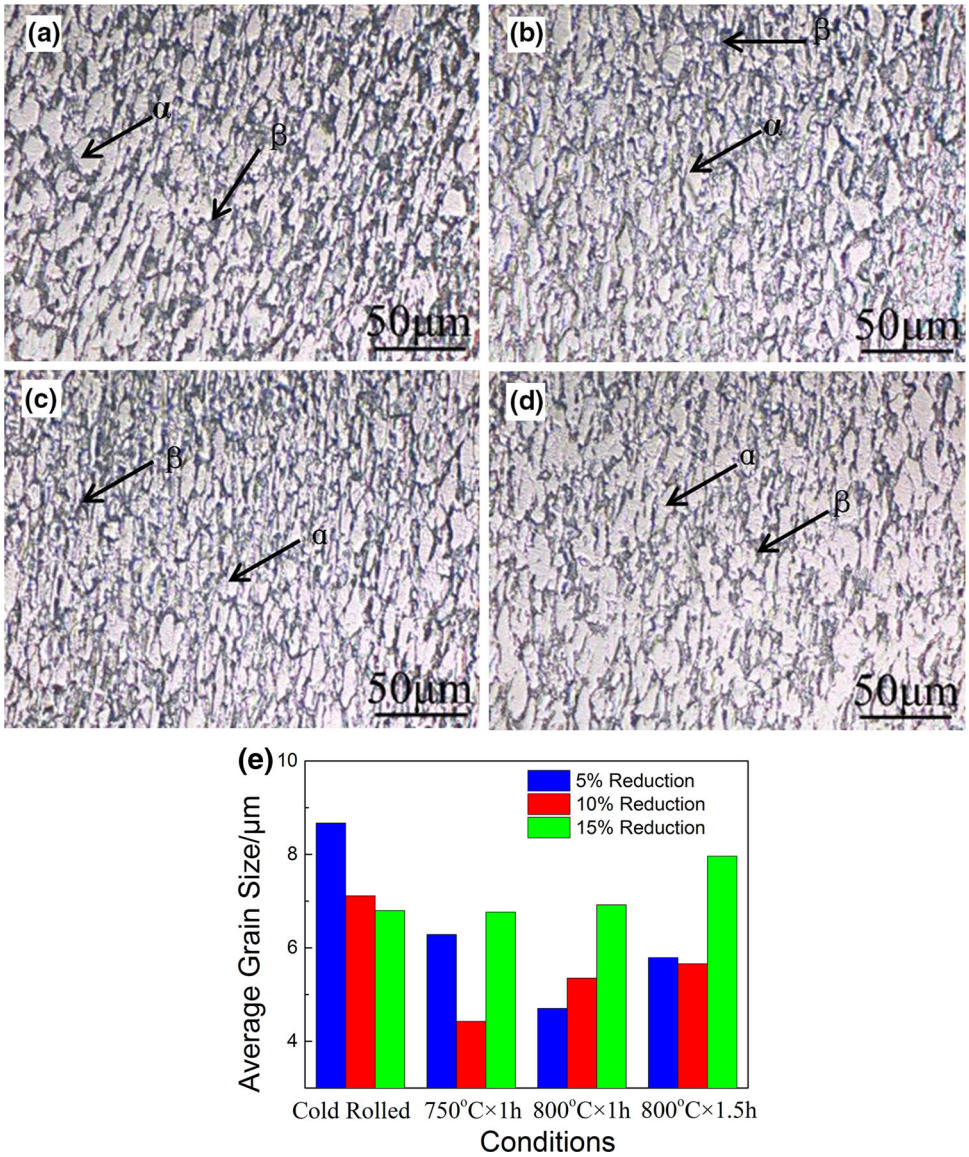

Fig. 1 The optical microstructures of (a) 5% cold-rolled plates, (b) 5% cold-rolled plate annealed at 800 °C for 1 h, (c) 10% cold-rolled plate annealed at 750 °C for 1 h, and (d) 10% cold-rolled plate annealed at 800 °C for 1 h, and the chart of (e) average grain size distribution

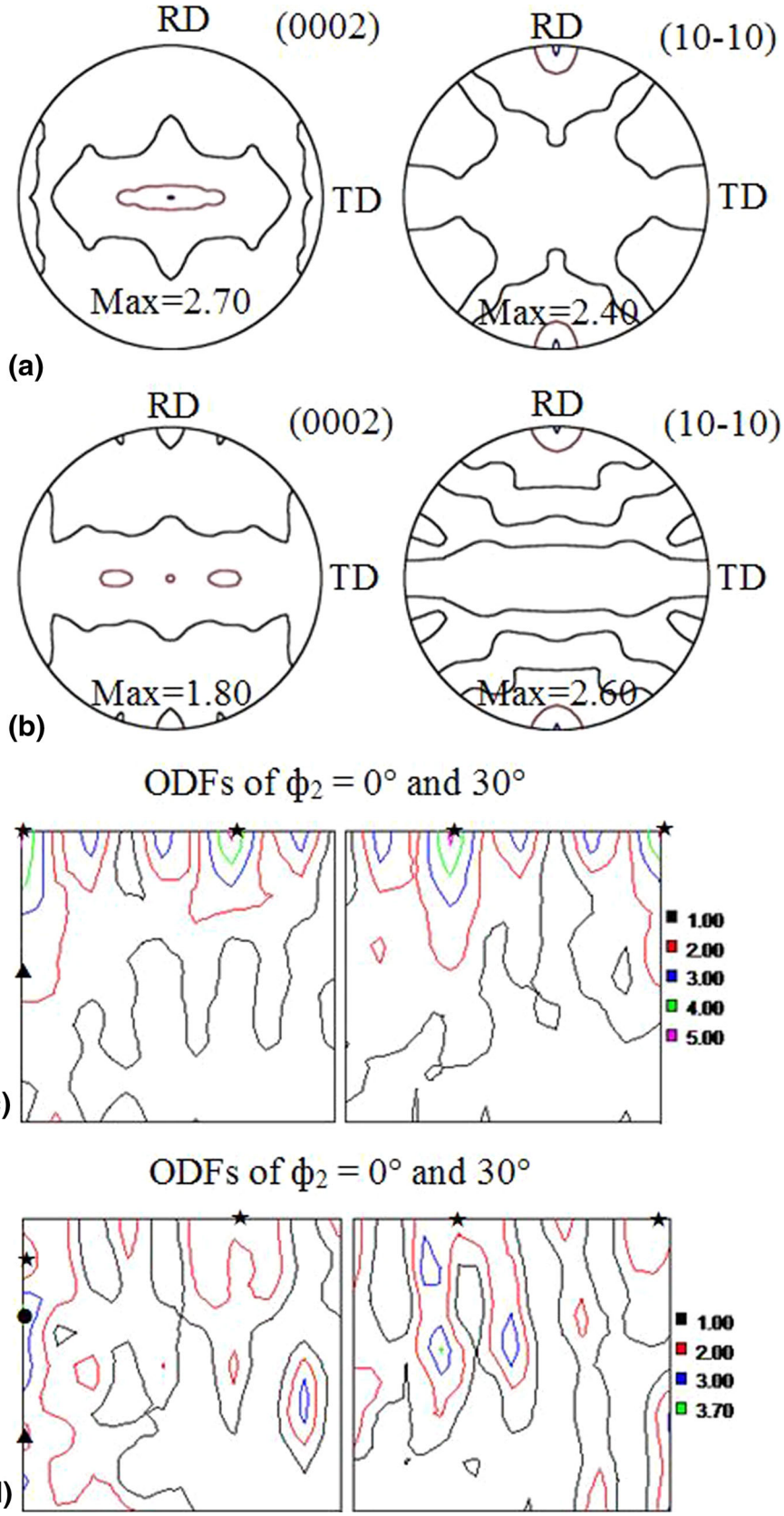

Fig. 2 Maximum intensity of (0002) and (10-10) pole figures of 10% cold-rolled plate (a) as received and (b) annealed at 750 °C for 1 h and the ODFs of constant ϕ2 in the 10% cold-rolled plates (c) as received, (d) annealed at 750 °C for 1 h, (e) annealed at 800 °C for 1 h and (f) annealed at 800 °C for 1.5 h. ★ stands for (0001) (Ref 10), ● for (01-12) (Ref 10), ◆ for (01-10) (Ref 10), and ▲ for (10-11) [1-210]

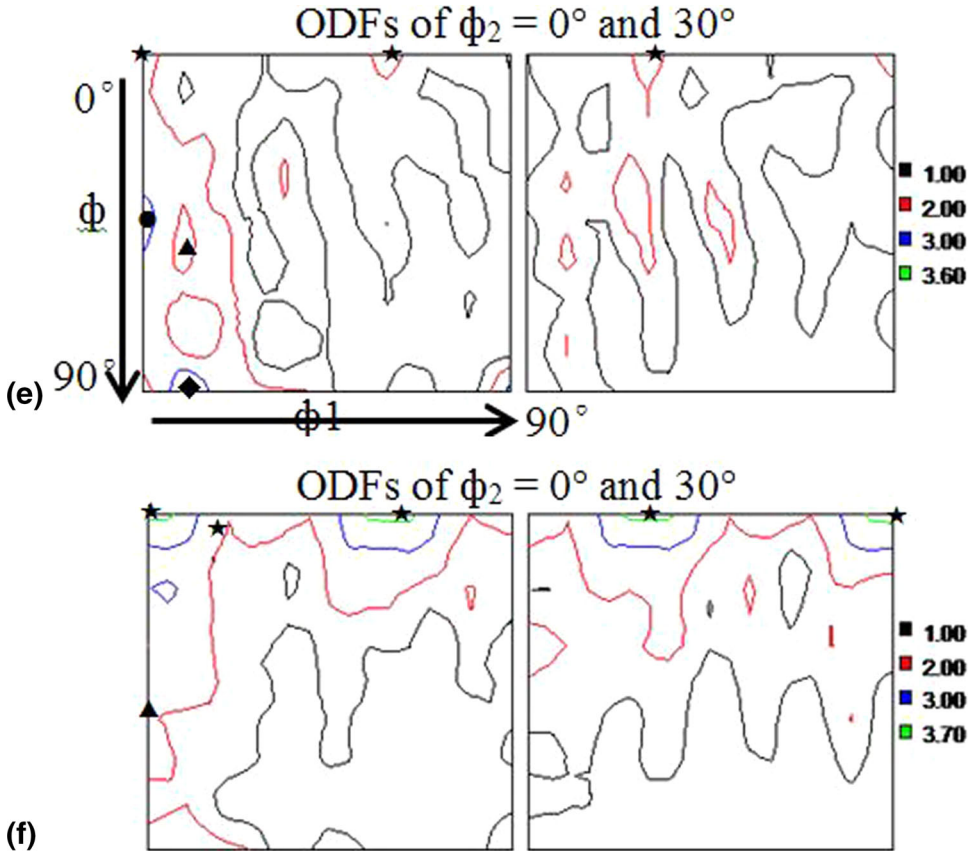

Fig. 2 continued

phases (Ref 11) which were elongated after deforming. It is apparently different from the equiaxed grains of the forged ingot that had an average grain size of 9.2 μm. Moreover, average grain sizes of three cold-rolled plates were 8.67 μm, 7.12 μm, and 6.80 μm, which showed a downward trend with increasing rolling reduction. Static recrystallization of α and β phases as well as β transformation during annealing process, contributed to grain refinement (Ref 12), as shown in Fig. 1(a) and (b).

The purpose of annealing is to acquire appropriate final microstructure through static recrystallization. Lenain et al. (Ref 13) studied the α phase nucleation and grain growth in a two-phase titanium alloy (Ti-LCB), finding out that α phase nucleated at the grain boundaries and even coalesced at several areas when annealed at 750 °C. At the same time, β phase decomposed due to α phase precipitation near the grain boundaries. Guo et al. (Ref 14) researched microstructure and texture evolution of the Ti-23Nb-0.7Ta-2Zr-1.2O alloy, a β-type titanium alloy which processes a higher recrystallization temperature. The samples after cold processing with a reduction ratio of 90% were subjected to different heat treatments at 800, 820, and 840 °C for 5, 10, 15, 20, and 30 min, respectively. At early stage of annealing at 800 °C, hardness decreased slightly within 20 min and then remained constant thereafter, which revealed a complete recrystallization process indirectly. Ivasishin et al. (Ref 15) researched grain growth and texture evolution of the Ti-6Al-4V alloy during continuous heating conditions in which the samples were heated to peak temperature, cooled to 800 °C, and held for 5 min. After being heated up to 1020 °C and then held at 800 °C for 5 min, the microstructure of sample exhibited an equiaxed grains and 6-8% beta phase was retained, which indicated a complete recrystallization. Ti-6Al-4V-0.1B alloy sheet with a thickness reduction of 90% was annealed at 900 °C. After 45 min, most of α grains globalized even though grain size varied a lot. These grains tended to grow, resulting from decrease in free energy that was due to reduction in total grain boundary area (Ref 16, 17). In view of the facts in the literature, the cold-rolled samples annealed at different temperatures for different durations were believed to complete static recrystallization process. The reason for the decrease of average grain size was the formation of recrystallized grains. However, the extension of time contributed to grain growth, leading to a slight increase in average grain size (Fig. 1e). Grain growth took place resulting in decrease in both boundary area/unit volume and stored energy/unit volume, and therefore, a high thermodynamic stability was achieved (Ref 18, 19). The microstructure of the 10% cold-rolled plate annealed at 750 °C for 1 h was refined dramatically although some grains elongated along rolling direction. Compared with the average grain size of the plate annealed at 750 °C for 1 h (4.43 μm), the average grain size of the plate annealed at 800 °C for 1 h increased to 5.35 μm (Fig. 1d), which indicated that recrystallization temperature declined with the increasing cold rolling reduction (Ref 20, 21). More refined microstructure and β phase were obtained with increasing annealing temperature (within 1 h). As shown in Fig. 1(a) and (d), due to the coarsening of primary α grains by Ostwald ripening where in small equiaxed α grains dissolve, coarser ones grew up, causing to decrease overall interfacial area (Ref 22, 23).

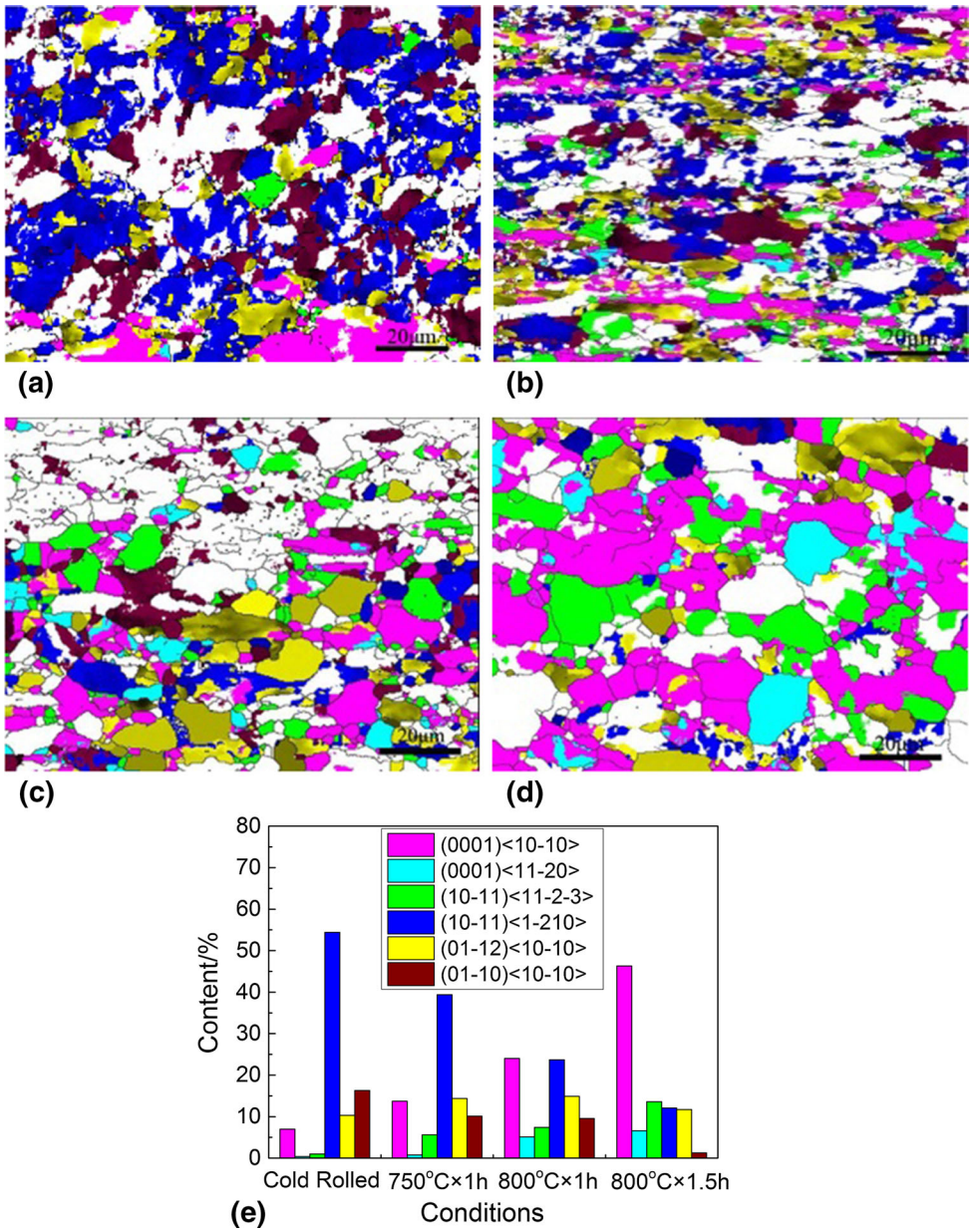

Fig. 3 Texture maps of the 10% cold-rolled plates (a) as received, (b) annealed at 750 °C for 1 h, (c) annealed at 800 °C for 1 h, (d) annealed at 800 °C for 1.5 h and (e) content chart

3.2 Texture Evolution

The (0002) complete pole figure (Fig. 2a) revealed a bimodal distribution of basal poles, a texture commonly found in titanium alloy. Cold-rolled texture and recrystallization texture are similar, and dispersed allocations were associated with relatively small rolling reductions (Ref 24). The maximum intensity of cold-rolled texture was 2.7 along the rolling direction, proving inhomogeneity between RD and TD. The values descended to 1.8 and 2.0 after annealing process at 750 °C for 1 h and 800 °C for 1 h, respectively. In the (10-10) pole figure, the maximum intensity was found along RD, suggesting that deformation texture developed during cold rolling. The influence of annealing conditions on the intensity of (10-10) pole figure was not as great as that of (0002) (Fig. 2a and b), which had a significant effect on homogeneity.

In order to analyze recrystallization and texture evolution of the samples, ODFs (Fig. 2) with a fixed ϕ_2 (0° and 30°) were obtained. Figure 2(c) reveals that the basal texture in specimen rolled with 10% reduction mainly consisted of components {0001} ⟨10-10⟩ and (10-11) ⟨1-210⟩. After annealing at 750 °C for 1 h, the maximum intensity of basal pole was at locations tilted 30° (±10°) from ND toward RD by ⟨10-10⟩, transforming to components {01-12}⟨10-10⟩. Recrystallization texture in the cold-rolled sample annealed at 800 °C for 1 h included strong {01-10}⟨10-10⟩ texture and weak {01-12}⟨10-10⟩ texture at locations tilted 45° from ND toward TD, which resulted from the weakening effect of recrystallization on texture (Ref 25). Nevertheless, strong {0001} ⟨10-10⟩ texture with maximum intensity of 2.8 similar to cold-rolled texture was found in the plate annealed at 800 °C for 1.5 h. This indicated that

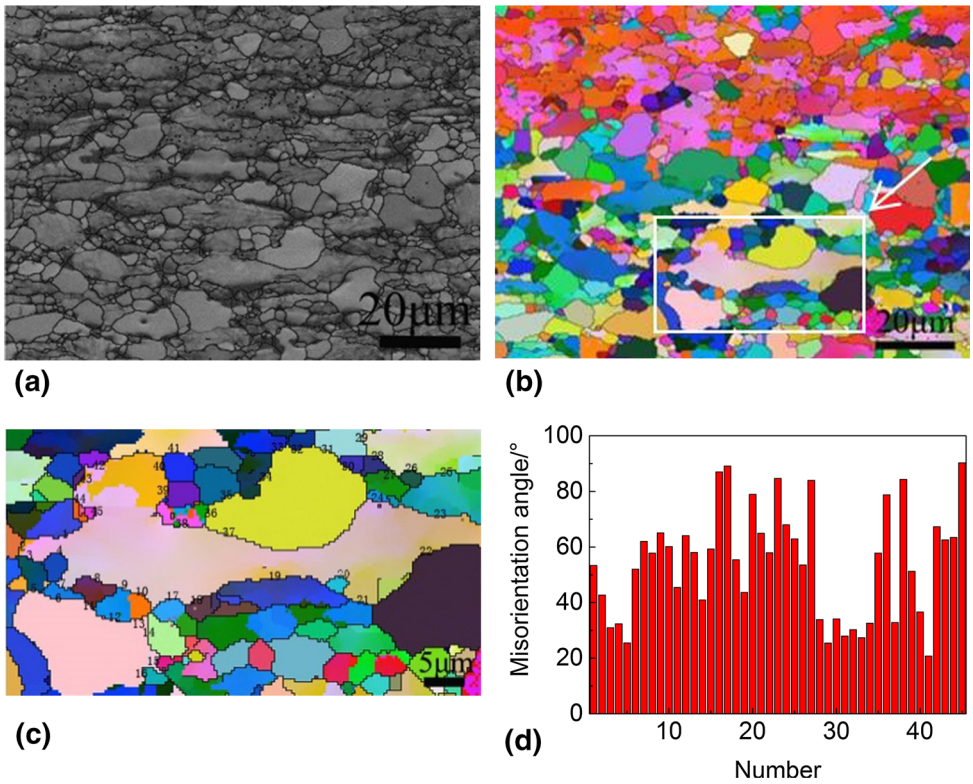

Fig. 4 Band contrast (a) and Euler (b) maps of the 10% cold-rolled plates annealed at 800 °C for 1 h, euler map (c) and (d) relative misorientation angles of the selected area (b)

extension of annealing time did not help alleviate cold-rolled texture (Ref 26).

EBSD results also verified that components {0001} ⟨10-10⟩, {10-11} ⟨1-210⟩, {01-10} ⟨10-10⟩, and {01-12} ⟨10-10⟩ play an important role in cold-rolled texture as well as recrystallization texture. The {0001}⟨10-10⟩ texture with a maximum intensity accounted for 6.98% in the cold-rolled plate, while component {10-11} ⟨1-210⟩ approximated 54.4% (Fig. 3e). It indicated that pyramidal slip system contributed to deformation in hexagonal metals and grains tended to arrange along ⟨1-210⟩ direction for maximum density (Ref 27). At the same time, weak components {01-12} ⟨10-10⟩ and {01-10} ⟨10-10⟩ were also developed during cold rolling. After recrystallization, the content of basal texture {0001} ⟨10-10⟩ varied slightly except in the plate annealed at 800 °C for 1.5 h, which accounted for 46.3%. Furthermore, {0001} ⟨11-20⟩ texture was enhanced up to 6.61% in the plate annealed at 800 °C for 1.5 h. Apparently, {10-11} ⟨1-210⟩ texture was reduced in the plate annealed at 750 and 800 °C for 1 h, especially in the latter one. Components {01-12} ⟨10-10⟩ and {01-10} ⟨10-10⟩ accounted for 14.4 and 10.1%, respectively, in the plate annealed at 750 °C for 1 h, which were nearly at the same level as of those in the plate annealed at 800 °C for 1 h. The fact that grains tended to be arranged along the ⟨10-10⟩ direction, parallel to the rolling direction, was obvious in the cold-rolled sample. However, EBSD result testified a downward trend of rolling texture with an increase of annealing time and/or temperature, as presented in Fig. 3(e). It was believed that the weakening of basal texture and pyramidal texture resulted in good comprehensive performance.

3.3 Recrystallization Mechanism

Recrystallization behavior of the Ti-6Al-4V alloy during annealing process was determined by several factors, i.e., original textures inherited from cold rolling process, grain nucleation sites, and its growth orientations. The EBSD maps (Fig. 4) suggested complete recrystallization in the Ti-6Al-4V alloy plate, annealed at 800 °C for 1 h. It was noted that grains with an average grain size of 15 μm were surrounded by dozens of recrystallized grains with an average grain size of 4 μm which were formed at the earlier stage of annealing treatment. Due to the interaction of dislocations and precipitates along grain boundaries, a large number of nucleation sites were formed (Ref 28). On the other hand, deformed grains provided nucleation sites, contributing to separation of original grains and the formation of recrystallized ones.

An area (Fig. 4b) was selected to further clarify the recrystallization mechanisms, and various numbers were marked in the grain boundaries between non-recrystallization grains and adjacent recrystallized ones. In the selected area, these recrystallized equiaxed grains formed particularly in the grain boundaries, with high energy (Ref 8). The misorientation angles (Fig. 4d) between neighboring grains all exceeded 15°, ranging from 20.8° to 90.3°. The dispersive misorientation angle distribution revealed a fact that the recrystallized grains mostly grew to different orientations. Therefore, the recrystallized nucleation sites with preferred orientations tended to grow to recrystallization texture with some preferred orientations later (Ref 29). The reason is that a 10% reduction resulted in the movement and entanglement of numerous dislocations (Ref

30), which then became the subgrain boundaries. Afterward, as recrystallization sites, these subgrains possibly with the same preferred orientations grew to the particular orientations.

The mechanism of favorable grain growth also played an important role in recrystallization texture. Compared with the cold-rolled textures, the textures in the annealed plate showed a clear transformation in which most grains in close-packed direction ⟨1-210⟩ were more likely to be arranged in ⟨10-10⟩ direction, leading to the reduction of component {10-11} ⟨1-210⟩ and the formation of components {01-10} ⟨10-10⟩ and {01-12} ⟨10-10⟩. The {01-10} ⟨10-10⟩ and {01-12} ⟨10-10⟩ textures which tilted 10° from RD toward TD, followed by 90° from ND toward TD and 45° from ND toward TD along ⟨10-10⟩ direction, respectively, were developed, forming 9.56% and 14.9%, respectively. These grains were more likely to grow up (Ref 20, 27), and thus, new textures were obtained during annealing process, which was the mechanism of grain growth in recrystallization.

4. Conclusions

The effect of recrystallization on microstructure and texture evolution of the cold-rolled Ti-6Al-4V alloy plates was investigated via OM, SEM, XRD, and EBSD. The following conclusions were drawn based on these experimental results. More refined microstructure and β phase are obtained with increasing annealing temperature (within 1 h). However, the extension of annealing time results in grain growth. The textures of the cold-rolled sample mainly consist of components {0001} ⟨10-10⟩, {10-11} ⟨1-210⟩, {01-12} ⟨10-10⟩, and {01-10} ⟨10-10⟩. The weak {10-11} ⟨1-210⟩ texture transformed to components {01-12} ⟨10-10⟩ and {01-10} ⟨10-10⟩, and the content of {10-11} ⟨11-2-3⟩ texture showed a slightly upward trend with extension of annealing time and/or temperature. The formation of pyramidal texture as well as prismatic surface texture in recrystallized specimens had significant influence on formability of the Ti-6Al-4V alloy. EBSD results indicated that two mechanisms including recrystallization grain nucleation sites with preferred orientations and favorable grain growth played decisive roles in recrystallization.

Acknowledgments

The work was financially supported by the "Project of annual 25000 tons special oil pipe with high strength and excellent corrosion resistance in Hengshui, Hebei." The assistance of Dr. X Li and Mr. Y Zhang is also appreciated especially for their experimental support and beneficial discussion.

References

1. P.H. Morton, Titanium Alloys for Engineering Structures, *Philos. Trans. R. Soc.*, 1976, **282**(1307), p 401–411
2. G.S. Wang and R.Z. Tian, *Application of Titanium*, 1st ed., Central South College Press, Changsha, 2007, p 101–103
3. O. Music, J.M. Allwood, and K. Kawai, A Review of the Mechanics of Metal Spinning, *J. Mater. Process. Technol.*, 2010, **210**(1), p 3–23
4. R.R. Boyer, Titanium for Aerospace: Rationale and Applications, *Adv. Perform. Mater.*, 1995, **2**(4), p 349–368
5. Y.B. Wang, Y.H. Zhao, Q. Lian, X.Z. Liao, R.Z. Valiev, S.P. Ringer, Y.T. Zhu, and E.J. Lavernia, Grain Size and Reversible Beta-to-Omega Phase Transformation in a Ti Alloy, *Scr. Mater.*, 2010, **63**(6), p 613–616
6. F. Li, J. Mo, J. Li, L. Huang, W. Fan, and J. Fang, Effects of Deformation Rate on Ductility of Ti-6Al-4V Material, *Proc. Eng.*, 2014, **81**, p 754–759
7. M. Zhan, Z.Q. Jiang, H. Yang, X.D. Xu, and G.J. Li, Numerically Controlled Bending Performance of Medium Strength TA18 Titanium Alloy Tubes Under Different Die Sets, *Sci. China Technol. Sci.*, 2011, **54**(4), p 841–852
8. B.S. Yilbas, S.S. Akhtar, A. Matthews, C. Karatas, and A. Leyland, Microstructure and Thermal Stress Distributions in Laser Carbonitriding Treatment of Ti-6Al-4V Alloy, *J. Manuf. Sci. E.*, 2011, **133**(2), p 379–399
9. Y.B. Chun, S.H. Yu, S.L. Semiatin, and S.K. Hwang, Effect of Deformation Twinning on Microstructure and Texture Evolution During Cold Rolling of CP-Titanium, *Mater. Sci. Eng. A*, 2005, **398**(1), p 209–219
10. X. Huang, K. Suzuki, M. Yuasa, and Y. Chino, Microstructural and Textural Evolution of Pure Titanium During Differential Speed Rolling and Subsequent Annealing, *J. Mater. Sci.*, 2014, **49**(8), p 3166–3176
11. C. Jeon, C.P. Kim, S.H. Joo, H.S. Kim, and S. Lee, High Tensile Ductility of Ti-Based Amorphous Matrix Composites Modified from Conventional Ti-6Al-4V Titanium Alloy, *Acta Mater.*, 2013, **61**(8), p 3012–3026
12. X. Peng, H. Guo, T. Wang, and Z. Yao, Effects of β Treatments on Microstructures and Mechanical Properties of TC4-DT Titanium Alloy, *Mater. Sci. Eng. A*, 2012, **53**, p 55–63
13. A. Lenain, N. Clément, P.J. Jacques, and M. Véron, Characterization of the α Phase Nucleation in a Two-Phase Metastable β Titanium Alloy, *J. Mater. Eng. Perform*, 2005, **14**(6), p 722–727
14. W.Y. Guo, H. Xing, J. Sun, X.L. Li, J.S. Wu, and R. Chen, Evolution of Microstructure and Texture During Recrystallization of the Cold-Swaged Ti-Nb-Ta-Zr-O Alloy, *Metall. Mater. Trans. A*, 2008, **39**(3), p 672–678
15. O.M. Ivasishin, S.L. Semiatin, P.E. Markovsky, S.V. Shevchenko, and S.V. Ulshin, Grain Growth and Texture Evolution in Ti-6Al-4V During Beta Annealing Under Continuous Heating Conditions, *Mater. Sci. Eng. A*, 2002, **337**(1), p 88–96
16. S. Roy, S. Karanth, and S. Suwas, Microstructure and Texture Evolution During Sub-transus Thermo-Mechanical Processing of Ti-6Al-4V-0.1 B Alloy: Part II. Static Annealing in (α + β) Regime, *Metall. Mater. Trans. A*, 2013, **44**(7), p 3322–3336
17. F.X. Gil, D. Rodriguez, and J.A. Planell, Grain Growth Kinetics of Pure Titanium, *Scr. Mater.*, 1995, **33**(8), p 1361–1366
18. F.J. Gil and J.A. Planell, Grain Growth Kinetic of The Near Alpha Titanium alloys, *J. Mater. Sci. Lett.*, 2000, **19**(22), p 2023–2024
19. F.J. Gil and J.A. Planell, Behavior of Normal Grain Growth Kinetics in Single Phase Titanium and Titanium Alloys, *Mater. Sci. Eng. A*, 2000, **283**(1), p 17–24
20. P.V. Neminathan, M.S. Velpari, S.R.A. Rao, and A.K. Gogia, Development of Ring Forgings in Ti-6Al-4V Alloy for Aero-engine Applications, *Trans. Indian Inst. Met.*, 2012, **61**(5), p 355–361
21. I. Lonardelli, N. Gey, H.R. Wenk, M. Humbert, S.C. Vogel, and L. Lutterotti, In Situ Observation of Texture Evolution During α → β and β → α Phase Transformations in Titanium Alloys Investigated by Neutron Diffraction, *Acta Mater.*, 2007, **55**(17), p 5718–5727
22. S.L. Semiatin, B.C. Kirby, and G.A. Salishchev, Coarsening Behavior of an Alpha-Beta Titanium Alloy, *Metall. Mater. Trans. A*, 2004, **35**(9), p 2809–2819
23. S. Roy and S. Suwas, Microstructure and Texture Evolution During Sub-transus Thermomechanical Processing of Ti-6Al-4V-0.1 B Alloy: Part I. Hot Rolling in (α + β) Phase Field, *Metall. Mater. Trans. A*, 2013, **44**(7), p 3303–3321
24. Z.S. Zhu, J.L. Gu, R.Y. Liu, N.P. Chen, and M.G. Yan, Variant Selection and Its Effect on Phase Transformation Textures in Cold Rolled Titanium Sheet, *Mater. Sci. Eng. A*, 2000, **280**(1), p 199–203
25. S.V. Zherebtsov, G.S. Dyakonov, A.A. Salem, S.P. Malysheva, G.A. Salishchev, and S.L. Semiatin, Evolution of Grain and Subgrain Structure During Cold Rolling of Commercial-Purity Titanium, *Mater. Sci. Eng. A*, 2011, **528**(9), p 3474–3479
26. H.T. Jiang, X.Q. Yan, J.X. Liu, and X.G. Duan, Effect of Heat Treatment on Microstructure and Mechanical Property of Ti-Steel

Explosive-Rolling Clad Plate, *T. Nonferr. Met. Soc.*, 2014, **24**(3), p 697–704
27. Z.H. Chen, *Deformed Manganese Alloy*, 1st ed., Chemical Industry Press, China, 2005, p 58–63
28. Y.N. Yu, *Fundamentals of Materials Science*, 2nd ed., Higher Education Press, China, 2006, p 739–750
29. S.L. Semiatin, S.L. Knisley, P.N. Fagin, D.R. Barker, and F. Zhang, Microstructure Evolution During Alpha-Beta Heat Treatment of Ti-6Al-4V, *Metall. Mater. Trans. A*, 2003, **34**(10), p 2377–2386
30. T. Morita, K. Asakura, and C. Kagaya, Effect of Combination Treatment on Wear Resistance and Strength of Ti-6Al-4V alloy, *Mater. Sci. Eng. A*, 2014, **618**, p 438–446